doi:10.14311/ppt.2025.3.226
Plasma Physics and Technology **12**(3):226–232, 2025

STUDY OF THE BEHAVIOR OF AN ELECTRIC ARC DURING THE PASSAGE OF AN 8/20 µS IMPULSE CURRENT AND A FOLLOW CURRENT IN A SPARK GAP

O. M. D. RAZAFINDRASATA[a,b,*], P. FRETON[a], J.J GONZALEZ[a], C. D. PHAM[b], V. CREVENAT[b], Y. GANNAC[b]

[a] *Laboratoire plasma et conversion d'énergie (Laplace) UMR 5213 - CNRS - Toulouse INP - UT3 Université Toulouse 3 - Paul Sabatier 118, route de Narbonne - bât 3R3 – 31062 Toulouse cedex 9, France*

[b] *Département R&D, CITEL, 3 impasse de la blanchisserie, 51100 REIMS, France*

[*] razafindrasata@laplace.univ-tlse.fr

Abstract.

The technologies of spark gaps involve two distinct types of current: an impulse current that simulates a lightning strike and a follow current resulting from the persistence of the arc after the impulse. This study shows the behavior of the electric arc with 8/20 µs impulse current followed by a 200 A follow current, using both experiments and numerical tools. The geometry includes a pre-chamber, a main chamber (without separators), and an open outlet. We developed a three-dimensional (3D) numerical model to simulate the arc movement. This model is based on the assumption of local thermodynamic equilibrium (LTE) and operates under unsteady conditions. In our experiments, we use high-speed camera recordings and electrical measurements. A good agreement is observed between the numerical model and the experimental measurements, both in terms of arc shape and arc voltage values.

Keywords: model, spark gap, impulse current.

1. Introduction

The increasing integration of electronic components into electrical systems has significantly heightened their sensitivity to overvoltages. To ensure effective protection of low-voltage equipment against such surges, surge protective devices (SPDs) are commonly used. One of the key components that ensures the effectiveness of these devices is the use of nonlinear elements such as spark gaps. The role of the spark gap is to provide galvanic isolation in the absence of overvoltage, and to offer a conductive path to discharge excess energy to ground when an overvoltage occurs [1].

The spark gap consists of two electrodes separated by a small gap, ensuring galvanic isolation. One electrode is electrically connected to the phase to be protected, while the other is connected to the ground. When an overvoltage occurs, an electric arc is triggered between the two electrodes, creating a low-resistance conductive path. This channel temporarily short-circuits the phase to ground, allowing excess energy to safely be dissipated. After the lightning impulse has passed, the spark gap must return to its insulating state. However, the electric arc does not extinguish immediately, and a current continues to flow through the gap. This current, known as the "follow current", must be interrupted to prevent upstream protection devices from activating, which would otherwise disconnect the power supply system.

Over the years, various systems have been developed to limit this follow current [1–6]. In this study, we focus on a spark gap prototype that integrates an arc-splitting chamber [2, 4–6]. In order to effectively limit the current in such a device, the arc must move from its ignition zone to the chamber, where it can be segmented. It is therefore essential to investigate the physical phenomena that can influence this movement. However, the arc-splitting process itself will not be addressed in this work.

Additionally, two types of current are generally used when testing SPDs: an impulse current, representing the lightning strike, and a follow current, which persists after the impulse. According to standards [7], several impulse waveforms can be applied, such as 8/20 µs, 10/350 µs, or 10/1 000 µs. The first number refers to the rise time of the impulse to its peak, while the second corresponds to the time for the current to decay to half of its peak value. The duration of the follow current depends on the timing of the impulse relative to the mains voltage.

There are already previous studies focusing on air spark gaps equipped with arc-interruption chambers, subjected to different types of current impulses. Notably, the work of Ait-Amar [2] used a 10/350 µs, 14.5 kA impulse wave coupled to a 255 V – 50 Hz network. Both theoretical and experimental investigations were carried out. The theoretical study, conducted at LTE, was based on the magnetohydrodynamic (MHD) method without any specific treatment in the regions near the electrodes. On the experi-

mental side, voltage and current measurements were taken, along with high-speed camera recordings. This work mainly focused on the interruption capability of the device. Ait-Amar compared surge protection technologies using spark gaps with arc-splitting chambers to those using varistors. It was shown that components protected by varistor-based surge arresters are subjected to higher stresses due to a residual voltage that remains high for several milliseconds after the impulse.

One may also mention the work of Schneider [8], who used an 8/20 µs, 5 kA impulse wave, without follow current. The main objective was to validate the model by comparison with experimental results. The shapes and temporal positions of the arc observed by high-speed camera, as well as the voltage curves, were compared between the model and the experiment. The results showed good agreement between the two. The authors also emphasized the importance of mesh refinement to accurately represent the flow velocity, as well as the significant influence of plasma radiation data on hydrodynamic phenomena.

Our study proposes to investigate a simplified model of a spark gap equipped with an arc-splitting chamber (without separators), using an 8/20 µs current impulse followed by a follow current. We will study the transition between the impulse current and the follow current in order to assess its influence on the arc movement in a spark gap prototype we have designed. The objective is to compare the results obtained by our model with the experimental measurements, in order to validate it.

In this context, we will first present the numerical model and the geometric used. Next, we will describe the experimental setup. Finally, we will compare the results obtained from the simulation and experiment.

2. Model configuration

The work is dedicated to the design of a functional surge arrester prototype. Through the model, it is possible to access values of temperature, pressure, arc voltage, as well as other physical quantities. It also allows for the analysis of arc movement and all related phenomena.

The model we developed is based on the magnetohydrodynamics (MHD) approach, which couples the equations of fluid mechanics (mass, momentum, and energy conservation) with the electromagnetic equations. For numerical resolution, we use the commercial Ansys Fluent 2 023 software [9], which is based on the finite volume method (FVM). It allows for the development of User-Defined Functions (UDFs) to integrate thermodynamic, transport, and radiative properties as functions of temperature and pressure [10]. These properties were obtained from internal calculations carried out by the team. The properties used are those of air.

Source terms in the conservation equations, such as the Lorentz force (in the momentum equation), Joule heating, and radiative losses (in the energy equation), are also integrated using these UDFs.

Initial assumptions and geometry have been defined. The following paragraphs will present the details.

2.1. Hypotheses

The plasma is modeled under the assumption of local thermodynamic equilibrium (LTE), which allows the use of only one energy equation to represent the temperature of the medium. The flow is assumed to be laminar, and the fluid is simulated in a transient three-dimensional (3D) configuration. According to experimental results we assume that the vapours erosion is weak. So a pure Air medium is considered for the calculation of the plasma properties. The radiation will be taken into account using the net emission coefficient [11] calculated with a sphere radius of 5 mm.

A specific treatment was applied to the regions near the electrodes. These areas exhibit significant voltage drops and may also deviate from the equilibrium assumption. However, since LTE is assumed within the plasma medium, explicitly modeling a non-equilibrium zone would be a particularly demanding task. To overcome this difficulty, we implemented a resistivity model based on the work of Lindmayer [12]. This method consists in imposing an effective conductivity in the regions near the electrodes, defined by the following equation:

$$\sigma_{\text{eff}} = J \frac{\Delta y}{\Delta U} \tag{1}$$

where J is the current density, Δy the sheath thickness (0.1 mm), and ΔU a voltage drop derived from experimental measurements performed on copper separators as a function of the current density [12]. This method allows for the inclusion of an additional voltage drop when current passes through the material, in addition to that of the arc column.

Regarding the use of an 8/20 µs current impulse, the strong current variation over a short period of time led us to reassess the Ohm's law equation used in the model. The generalized form of Ohm's law is as follows:

$$\mathbf{E} + \mathbf{v} \times \mathbf{B} = \frac{\mathbf{J}}{\sigma} - \frac{\mathbf{J} \times \mathbf{B}}{n_{\text{e}} e} + \frac{\nabla_{\text{e}} P_{\text{e}}}{n_{\text{e}} e} + \frac{m_{\text{e}}}{n_{\text{e}} e^2} \frac{\partial \mathbf{J}}{\partial t} \tag{2}$$

Where $\mathbf{E}$: electric field, $\mathbf{v} \times \mathbf{B}$: electromotive field, $\frac{\mathbf{J}}{\sigma}$: resistive term, $\frac{\mathbf{J} \times \mathbf{B}}{n_{\text{e}} e}$: Hall term, $\frac{\nabla_{\text{e}} P_{\text{e}}}{n_{\text{e}} e}$: electron pressure, $\frac{m_{\text{e}}}{n_{\text{e}} e^2} \frac{\partial \mathbf{J}}{\partial t}$: electron inertia, σ: electrical conductivity, $\mathbf{B}$: magnetic field, n_{e}: electron density, e: electron charge, m_{e} electron mass.

The goal is to compare each term in this expression with the resistive term. The results showed that all terms were negligible for a current amplitude of 5 kA, in the context of an 8/20 µs wave. However, beyond 5 kA, the term related to the Hall effect becomes non-negligible and may need to be considered. Ultimately, all terms are negligible compared to the resistive term; thus, only this term and the electric field $\mathbf{E}$ remain in

equation 2. We retain the simplified form of Ohm's law, as seen in the work of [6, 8, 10]:

$$\mathbf{J} = \sigma \mathbf{E} \tag{3}$$

The conservation equations and electromagnetic equations used are widely documented in the literature [10, 13–16], and will therefore not be detailed in this article.

Finally, arc initiation is not modeled as a dielectric breakdown. Instead, it is modeled as a "fuse wire" type ignition, that is, an initially defined channel with high electrical conductivity. In our case, an arbitrary temperature of 15 kK at atmospheric pressure was imposed to initiate the conductive channel, allowing for sufficient electrical conductivity ($\sigma \approx 8.156$ S/m) to sustain the discharge.

2.2. Geometry

It includes an ignition zone with an inter-electrode distance of 1 mm, as well as a chamber not yet equipped with separators, with a height of 10 mm. The width of the device is 7.5 mm, with an electrode thickness of 2 mm. The electrodes are arranged in such a way that they gradually open as they extend toward the chamber. The radius of curvature of the lower electrode is 8 mm, while that of the upper electrode is 15 mm. The area between the ignition zone and the chamber will be referred to as the pre-chamber. The device opens into an outlet, while the rear side is completely closed. The geometry configuration is illustrated in figure 1.

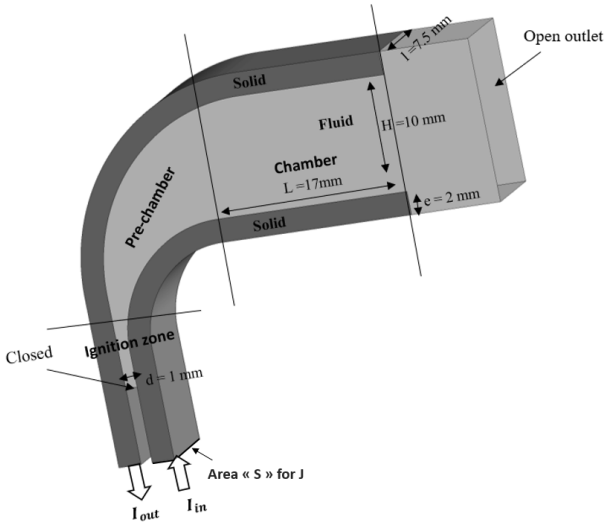

Figure 1. Geometry studied.

A mesh was constructed using hexahedral elements merged with a few tetrahedral. This mesh consists of approximately 850 000 cells, with a maximum cell size of 0.2 mm. According to Lowke and Tanaka [17], 0.1 mm layer was defined to represent the voltage drops caused by the anodic and cathodic sheaths.

To inject current into the electrodes, we applied a boundary condition with uniform current density (J = I/S) on the rear surface of the lower electrode (In), and a zero electric potential on the upper one. The current introduced into the model comes directly from experimental measurements.

We will now present the experimental setup we built, as well as the measuring instruments used.

3. Experimental setup

The experimental measurements consist of obtaining quantities that allow us to validate our model. The measurements carried out in this work mainly rely on high-speed camera imaging to capture the movement of the arc. Electrical measurements are also performed to compare the arc voltage value obtained by the model with that measured experimentally. The measurements were carried out on the same experimental setup.

The experimental setup was made using 3D printing to manufacture the casing (ABS material). It consists of two compartments designed to fit together. Two copper electrodes were machined independently from the casing to allow for easy replacement. A space was arranged on the lateral side to insert a glass window enabling visualization of the inside of the device. The experimental setup and the measurement circuit are shown in figure 2.

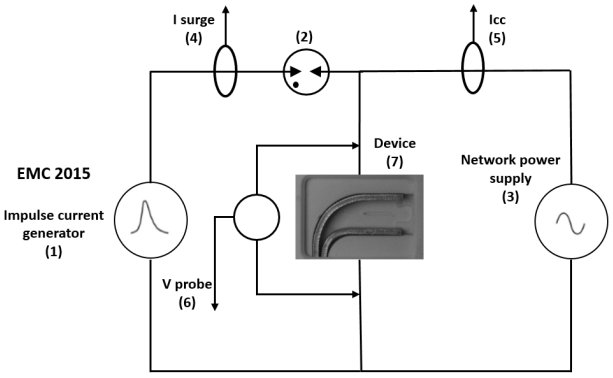

Figure 2. Measurement circuit.

The measurement circuit includes an EMC 2015 (1) generator (from HILO-TEST company) capable of delivering either an 8/20 µs current pulse (Imax = 23 kA) or a 10/1 000 µs current pulse (Imax = 200 A). In our case, we used the 8/20 µs pulse at 8 kA– 4 kV. A gas discharge tube (GDT) (2) is placed in series with the pulse generator to protect it in case of malfunction. We present here a schematic diagram. In practice, surge arresters were installed to protect the network, although they are not shown in this diagram. The different Pearson current probes (4) and (5) (Pearson current monitor model 101), which can measure up to 50 kA, measure respectively the surge current (Isurge) and the network current (Inetwork). For voltage measurements, a TT-SI 9010 voltage probe (6) was used, offering a measurement range from -7 000 V

to +7 000 V with a frequency of 100 MHz and an accuracy of ±2 %. The ±2 % accuracy refers to the measurement error: for example, for a voltage of 60 V measured by the probe, it corresponds to an error of 1.2 V.

To capture the arc movement, a Phantom Miro LAB310 high-speed camera equipped with a macro lens of 24-85 mm focal length was used. The aperture can be adjusted between f/2.8 and f/22. The camera can reach a maximum resolution of 1 280×800 at 3 200 fps. The resolution used in our measurements was 256×128 to achieve a frame rate of 77 000 fps. This choice was made after several tests to balance resolution and frame rate. We concluded that this is the minimum resolution that can be used to avoid overly pixelated images while still allowing observation of the arc at the pulse's peak amplitude, half-decay, and pulse end. Due to the high brightness of the arc, an attenuation filter of 1x1 000 was used.

Finally, the circuit is coupled with a mains power supply (3) of 255 Vac at 50 Hz frequency and a short-circuit current limited to 200 A. The generator is equipped with a system that can synchronize the two power supplies and trigger shots from 0 ° to 360 ° of the current cycle. We configured the circuit so that the 8/20 µs current impulse is always applied at the peak of the positive half-cycle (90 ° phase angle). Thus, each shot reproduces the same current waveform. The experimentally measured currents can be seen in figure 3.

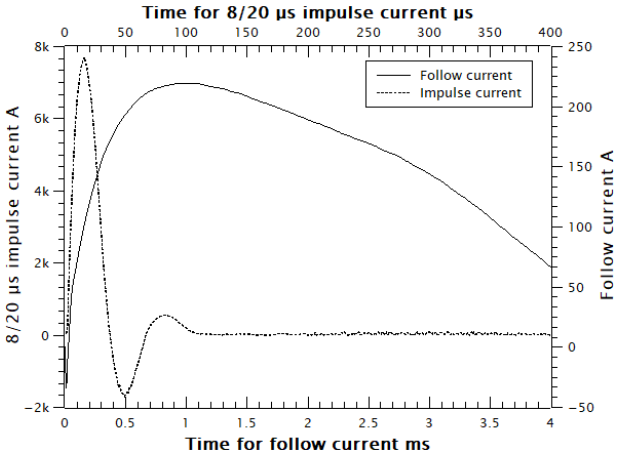

Figure 3. Currents from experimental measurements.

The current pulse can be seen lasting for 50 µs, with the current reaching its peak amplitude around 10 µs. Additionally, a current flows simultaneously with the pulse, lasting for 5 ms with an amplitude of 200 A, which is the follow current. Now, we will present and discuss the results obtained.

4. Results and discussion

Figures 4 and 5 present a comparison between the results obtained from the numerical model and those from the experimental measurements.

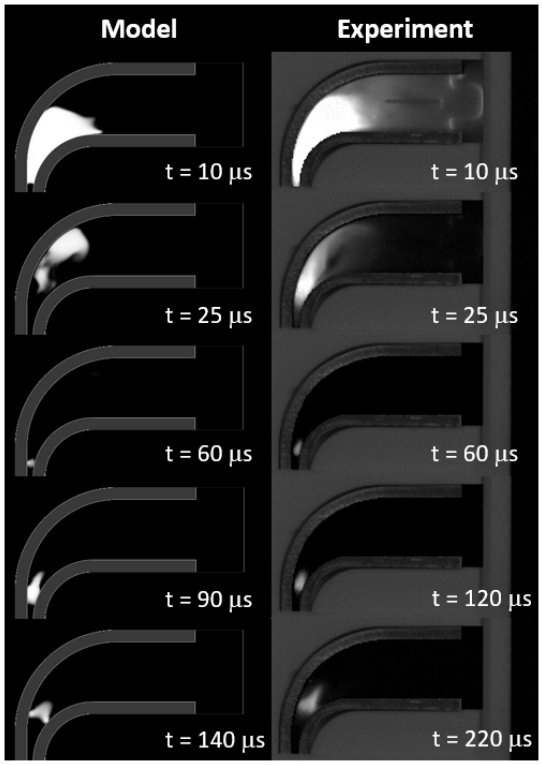

Figure 4. Comparison between the results obtained from the model (iso-temperature 10 kK) and the experiment (high-speed camera) with a current pulse + follow current – part 1.

The contours represent iso-temperature 10 kK. This contour level in the figures is compared with a certain level brightness of the video images. The comparison between the model and the experiment is not made at the same times but rather based on shape similarities at different times. At this temperature the electrical plasma conductivity is enought to assume a current path. So even if different physical effects may cause similar brightness we assume that this iso-temperature gives an indirect representation of arc plasma shape.

The first image shows the propagation of the arc at the moment when the current pulse reaches its peak (t = 10 µs). Based on experimental observations, it is noted that the light emitted by the arc is extremely intense, making it difficult to precisely distinguish the area actually occupied by the electric arc. The images show a bright flash that fills the entire rear part of the device, including the 1 mm inter-electrode gap (ignition zone). In contrast, with the numerical model, we were able to generate iso-temperature 10 kK, allowing us to identify the cells where the temperature is high enough to correspond to the presence of the arc. We assumed that this contour represents the volume effectively occupied by the arc plasma. This view revealed that the arc does not fully occupy the rear part of the device. Naturally, it is pushed forward toward the pre-chamber due to pressure forces and magnetic forces.

As the current decreases, the arc size also shrinks, as

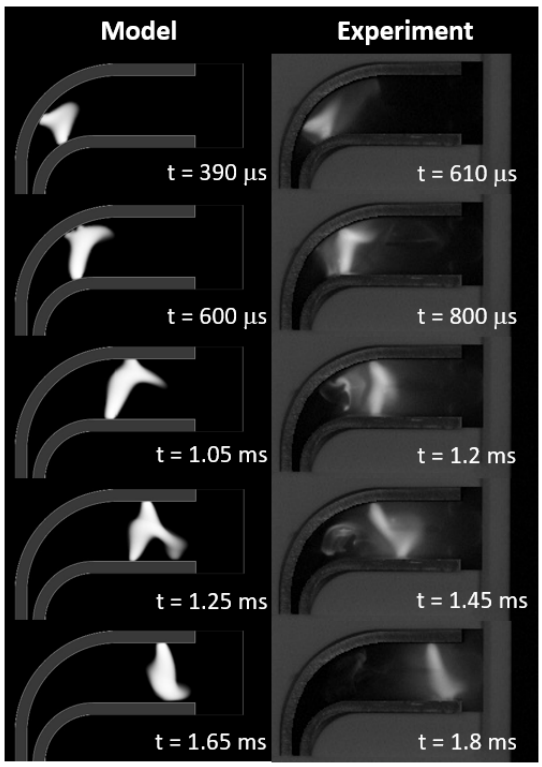

Figure 5. Comparison between the results obtained from the model (iso-temperature 10 kK) and the experiment (high-speed camera) with a current pulse + follow current – part 2.

seen at t = 25 µs. Thus, the most heated areas during the impulse are located in the pre-chamber, making it a favorable location for arc re-ignition. These regions retain a high temperature, and therefore a high electrical conductivity, facilitating current flow. This is observed at t = 60 µs, where the arc is still present and located at the entrance of the pre-chamber.

This positioning of the arc is a crucial factor, because if re-ignition occurs in the inter-electrode region (ignition zone), it would delay its movement: the arc would then have to travel a longer distance to reach the chamber. On the other hand, if re-ignition takes place in the pre-chamber, access to the chamber will be faster.

Subsequently, between t = 90 µs and t = 800 µs, the arc moves and stretches toward the chamber, still under the effect of pressure and magnetic forces. Due to the geometry of the device, the curved part of the arc column heats a portion of the upper electrode. This phenomenon is visible at t = 390 µs in the model and at t = 610 µs in the experiment. This localized heating leads to the formation of a new arc root (model: t = 600 µs, experiment: t = 800 µs), causing a stepwise movement of the arc. Finally, between t = 1 ms and t = 1.8 ms, the arc continues to move inside the chamber, gradually stretching with an overall uniform motion.

By comparing the shape of the arc observed in the model and in the experiment, we can see that they are similar. Indeed, there is preheating during the current pulse, the arc positioning in the pre-chamber at the end of the pulse, followed by its movement toward the chamber, and finally a fairly uniform movement inside the chamber. However, a slight time lag is observed regarding the arc displacement during the follow current phase. The model leads the experiment by approximately ±200 µs.

This lag could be explained by the experimental conditions. The experimental setup consists of two interlocking compartments, with gaps designed to hold the electrodes and a side window. This setup may potentially cause air leaks, influencing the arc's behavior. In contrast, in the numerical model, the geometry is considered perfectly sealed. During the current pulse the arc behavior seems to be driven mainly by the pressure forces (t < 50 µs), then the Lorentz forces act to push the arc to the chamber.

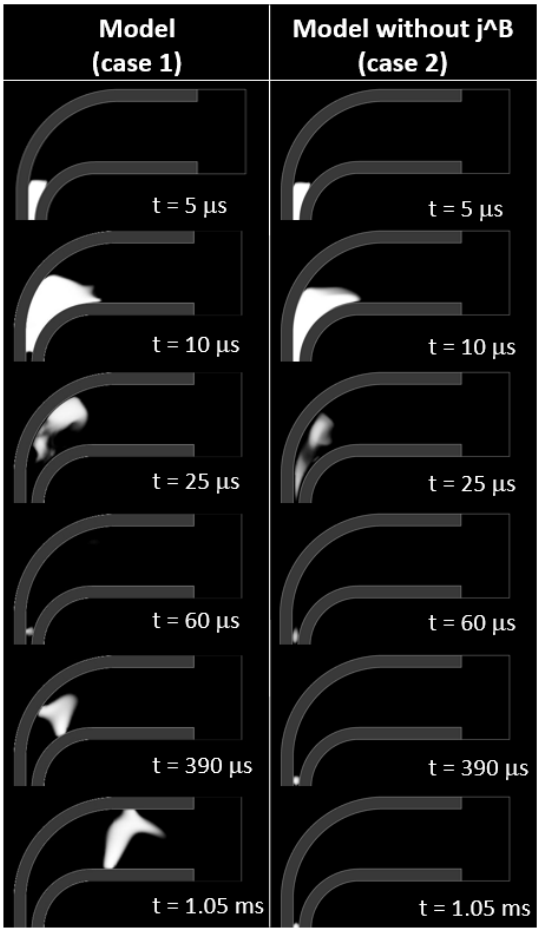

Figure 6. Influence of magnetic forces on arc movement.

To verify this physical point, we compared two more cases to observe the influence of the Lorentz forces. figure 6 shows the comparison between a model that accounts for both the pressure force and the magnetic force (case 1), and a model that considers only the pressure force (case 2). It is observed that, during the rise of the current impulse (t = 5 µs, t = 10 µs), the shape and movement of the electric arc remain similar

in both cases. A slight difference appears when the current starts to decrease, at times t = 25 µs and t = 60 µs. When the follow current takes over, in case 1, the arc continues its movement toward the chamber, whereas in case 2, it remains fixed in place (t = 390 µs, t = 1.05 ms).

Even if during the impulse current the pre heating of the chamber is similar in both case, without Lorentz forces the pressure is not enough then to follow to push the arc in the geometry. Applying or not the Lorentz forces during the impulse current leads to the same behavior showing the weak effect of the Lorentz forces. On contrary during the follow current these forces are essential and without their application the arc keeps to the ignition zone.

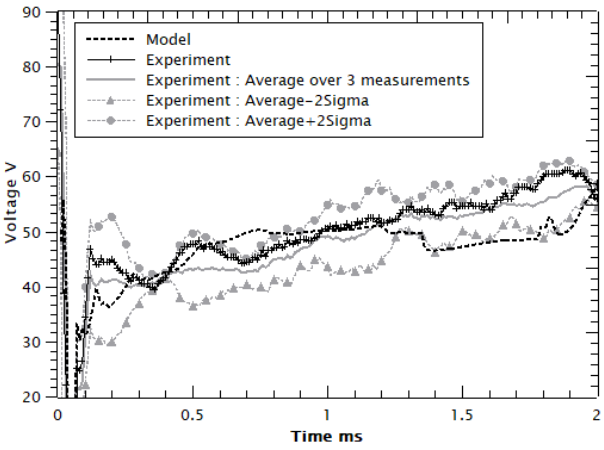

Figure 7. Comparison of the voltage obtained from the model and the experiment.

Figure 7 presents a comparison between the voltage obtained from the numerical model and that from the experimental measurements. The experimental curve corresponds to the average of three voltage measurements. To account for data variability, an envelope was constructed based on the bounds "Average ± 2Sigma", where Sigma represents the standard deviation of the measurements. This representation makes it possible to visualize how well the model results fall within the range of variation of the experimental data. Regarding the arc voltage, the results obtained by the model fall within the experimental envelope. A voltage of about 40 V is observed up to 700 µs, which gradually increases as the arc stretches, reaching a value between 45 V and 50 V once the arc is inside the chamber.

5. Conclusion

We have used a three-dimensional model able to represent the behavior of an electric arc during the transition from 8/20 µs pulse to the 200 A follow current. The arc transition phases are characterized by a preheating of the pre-chamber during the current impulse, followed by the establishment of an electric arc that remains ignited at the end of the impulse. The arc then elongates as it moves toward the chamber, where it eventually propagates by jumping.

It has been shown that the pressure force is more influential than the magnetic force during the current impulse, while conversely, the magnetic force becomes predominant during the follow current.

Observations of the behavior, trend, and value of the arc voltage show that the model is in good agreement with the experimental results. With a view toward a potential study of arc splitting, the model is able to reproduce the voltage rise due to arc elongation, as well as restrike phenomena.

References

[1] G. Finis, M. Wetter, and T. Meyer. New spark-gap technology with efficient line-follow current suppression for the protection of powerful LV distribution systems. *Surge Protection D-32825 Blomberg, Germany*, 2016. doi:10.1109/ICLP.2016.7791513.

[2] S. Ait-Amar, J. B. Ducourneau, and G. Serrie. Arc extinguishing method of SPD type 1. *IEEE Transactions on Dielectrics and Electrical Insulation*, 16(3), 2009. doi:10.1109/TDEI.2009.5128510.

[3] Y. Gannac, G. Leduc, C. D. Pham, and V. Crevenat. 8/20 and 10/350 surges behaviour of a gas discharge tube according to gas pressure. *Electric Power Systems Research*, 2021. doi:10.1016/j.epsr.2021.107302.

[4] A. Ehrhardt, S. Schreiter, and L. Huttner. Basic problems and solution of the encapsulation of a low–voltage spark gap with arc splitter chamber. *Journal of Electrical Engineering*, 63(2):103–108, 2012. doi:10.2478/v10187-012-0015-9.

[5] A. Ehrhardt and S. Beier. New deion chamber for encapsulated switchgear. In *ICEC, The 27th International Conference on Electrical Contacts*, 2014.

[6] A. Ehrhardt and O. Schneider. Surge protection device digital prototyping. In *ICEC 2020 – 30th International Conference on Electrical Contacts*, 2020.

[7] I. 61643-11:. *Low-voltage surge protective devices - Part 11: Surge protective devices connected to AC low-voltage power systems - Requirements and test methods*, 2025.

[8] O. Schneider, D. Gonzalez, and A. Ehrhardt. Multiphysical simulation of impulse current arcs in spark gaps for industrial applications. *Plasma Physics and Technology*, 10(3):119–122, 2023. doi:10.14311/ppt.2023.3.119.

[9] ANSYS. *Ansys Fluent Theory Guide Release 2023 R2.*

[10] P. Freton, J. J. Gonzalez, M. Masquere, and F. Reichert. Magnetic field approaches in DC thermal plasma modelling. *J. Phys. D: Appl. Phys.*, 44:345202, 2011. doi:10.1088/0022-3727/44/34/345202.

[11] Y. Naghizadeh-Kashani, Y. Cressault, and A. Gleizes. Net emission coefficient of air thermal plasmas. *J. Phys. D: Appl. Phys.*, 35:2925, 2002. doi:10.1088/0022-3727/35/22/306.

[12] A. Mutzke, T. Rüther, M. Lindmayer, and M. Kurrat. Arc behavior in low-voltage arc chambers. *EPJ Appl. Phys.*, 49(2), 2010. doi:10.1051/epjap/2010001.

[13] X. Li, D. Chen, Q. Wang, and Z. Li. Simulation of the effect of several factors on arc behavior in low voltage circuit breaker. *Plasma Sci & Technol*, 2005. doi:10.1088/1009-0630/7/5/022.

[14] B. Swierczynski, J. J. Gonzalez, P. Teulet, et al. Advances in low-voltage circuit breaker modelling. *J Phys D*, 37(4):595, 2004. doi:10.1088/0022-3727/37/4/011.

[15] X. Li. Study of the effect of gassing material on arc behavior in low voltage circuit breaker. *IEICE TRANS. ELECTRON.*, E90–C(7), 2007. doi:10.1093/ietele/e90-c.7.1460.

[16] F. Yang, M. Rong, Y. Wu, et al. Numerical analysis of the influence of splitter-plate erosion on an air arc in the quenching chamber of a low-voltage circuit breaker. *J. Phys. D: Appl. Phys.*, 43:434011, 2010. doi:10.1088/0022-3727/43/43/434011.

[17] J. J. Lowke and M. Tanaka. LTE-diffusion approximation for arc calculations. *J. Phys. D: Appl. Phys*, 39(16):3634, 2006. doi:10.1088/0022-3727/39/16/017.